ORIGINAL RESEARCH - PRECLINICAL

Micronized Acellular Matrix Biomaterial Leverages Eosinophils for Postinfarct Cardiac Repair

Vishnu Vasanthan, MD,[a] Ali Fatehi Hassanabad, MD, MSc,[a] Darrell Belke, PhD,[a] Guoqi Teng, PhD,[a]
Carmina Albertine Isidoro, BHSc,[a,b] Devjyoti Dutta, BSc,[a] Jeannine Turnbull, BSc,[a] Justin F. Deniset, PhD,[a,b,*]
Paul W.M. Fedak, MD, PhD[a,*]

VISUAL ABSTRACT

Vasanthan V, et al. J Am Coll Cardiol Basic Trans Science. 2023;8(8):939–954.
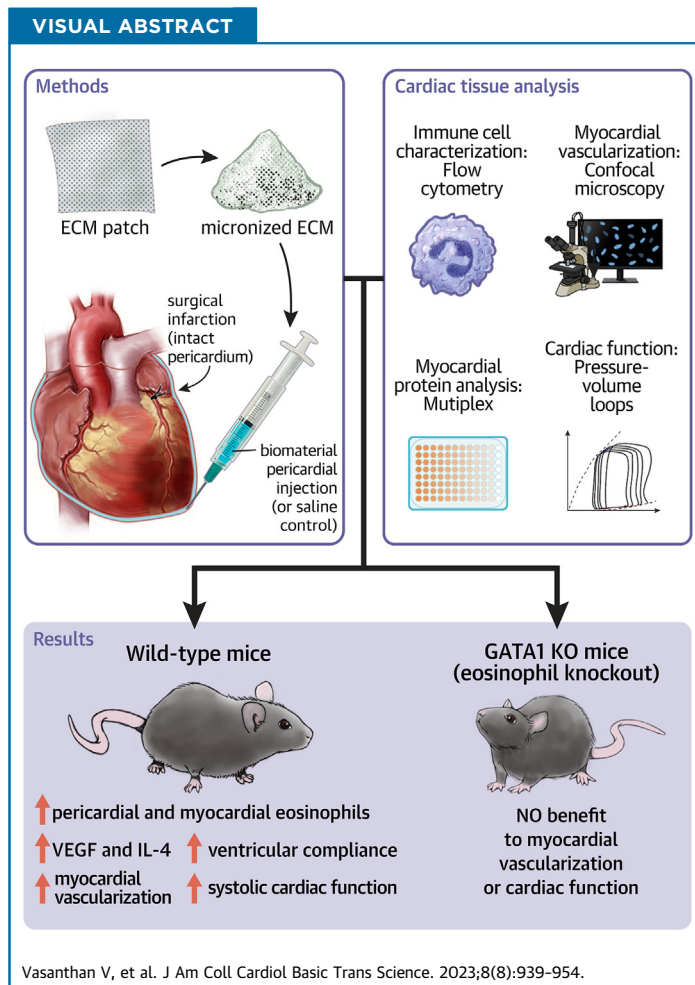
HIGHLIGHTS

- A micronized acellular matrix biomaterial redirects pericardial and myocardial inflammation to stimulate adaptive postinfarct cardiac repair mechanisms.

- Pericardial delivery of the micronized biomaterial increases pericardial and myocardial eosinophil counts in a small animal experimental MI model.

- The matrix biomaterial increases myocardial concentrations of pro-reparative IL-4 and VEGF proteins.

- The acellular matrix biomaterial increases neovascularization in the myocardial border zone and preserves postinfarct cardiac function.

- Genetic depletion of eosinophils using a knockout mouse model negates biomaterial-mediated benefits to neo-vascularization and cardiac function, demonstrating that eosinophils may play a critical role in biomaterial-mediated cardiac repair.

From the [a]Department of Cardiac Sciences, Libin Cardiovascular Institute, Cumming School of Medicine, University of Calgary,
Calgary, Alberta, Canada; and the [b]Department of Physiology and Pharmacology, University of Calgary, Calgary, Alberta, Canada.
*Drs Fedak and Deniset contributed equally to this work and are joint senior authors.

ABBREVIATIONS AND ACRONYMS

CM = biomaterial-conditioned media

DMEM = Dulbecco's modified Eagle medium

G = gauge

IHD = ischemic heart disease

IL = interleukin

KO = knockout

MI = myocardial infarction

mSIS-ECM = micronized porcine small intestinal submucosal extracellular matrix

PBS = phosphate-buffered saline

SIS-ECM = porcine small intestinal submucosal extracellular matrix

SMA = smooth muscle actin

TGF = transforming growth factor

Th = T helper

VEGF = vasculogenic endothelial growth factor

WT = wild type

SUMMARY

After ischemic injury, immune cells mediate maladaptive cardiac remodeling. Extracellular matrix biomaterials may redirect inflammation toward repair. Pericardial fluid contains pro-reparative immune cells, potentially leverageable by biomaterials. Herein, we explore how pericardial delivery of a micronized extracellular matrix biomaterial affects cardiac healing. In noninfarcted mice, pericardial delivery increases pericardial and myocardial eosinophil counts. This response is sustained after myocardial infarction, stimulating an interleukin 4 rich milieu. Ultimately, the biomaterial improves postinfarct vascularization and cardiac function; and eosinophil-knockout negates these benefits. For the first time, to our knowledge, we demonstrate the therapeutic potential of pericardial biomaterial delivery and the eosinophil's critical role in biomaterial-mediated postinfarct repair. (J Am Coll Cardiol Basic Trans Science 2023;8:939–954) © 2023 The Authors. Published by Elsevier on behalf of the American College of Cardiology Foundation. This is an open access article under the CC BY-NC-ND license (http://creativecommons.org/licenses/by-nc-nd/4.0/).

I schemic heart disease (IHD) remains a major cause of mortality.[1] Myocardial infarction (MI) can progress to end-stage heart failure, necessitating 38% of cardiac transplantations worldwide.[2,3] Contemporary IHD therapy focuses on restoring perfusion of damaged muscle and medical optimization, but there is no targeted therapy to enhance cardiac healing at the cellular level.[4-7] Postinfarct tissue healing is mediated by a complex interplay of immune cells and fibroblasts, whose phenotypes determine the balance between cardiac tissue fibrosis with resultant loss of function and myocardial angiogenesis with functional recovery of the injured tissues.[8] Developing targeted strategies to modulate cellular activity for adaptive angiogenic tissue healing may preserve cardiac function and further improve patient outcomes.

Acellular extracellular matrix biomaterials may bridge this therapeutic gap because they have been shown to promote endogenous mechanisms of adaptive cardiac repair.[6,7,9,10] Applied as an epicardial sheet in animal models of IHD, porcine small intestinal submucosal extracellular matrix (SIS-ECM) promotes a vasculogenic phenotype in cardiac fibroblasts and improves myocardial function and angiogenesis.[11-21] After MI, selected immune cell populations mediate debris clearance, extracellular matrix disruption, and the release of profibrotic molecules, and other pro-reparative immune cells facilitate angiogenesis and adaptive tissue healing.[13,20-26] SIS-ECM has recently demonstrated immunomodulatory properties by increasing myocardial proangiogenic neutrophil and monocyte content and subsequently promoting neovascularization.[24] In a human clinical pilot, epicardial application of SIS-ECM during coronary artery bypass surgery shows evidence of improved regional myocardial perfusion.[12] Epicardial biomaterial implantation, placed over the region of tissue injury, is feasible for patients receiving open-chest surgical revascularization.[12] Provided that its bioinductivity is maintained, micronizing SIS-ECM into an injectable form may add versatility to expand the eligible patient population to nonsurgical IHD patients. Targeted injectable therapies tend to focus on intramyocardial delivery; however, a novel pericardial strategy can uniquely leverage the reparative properties of the intact pericardial space.[27-31]

The pericardium contains reparative immune cell populations such as eosinophils and GATA6$^+$ macrophages.[25,26,32] Characterizing how biomaterials modulate pericardial immune responses and whether they enrich for reparative immune populations to influence healing remains unexplored and may uncover therapeutic targets by defining new mechanisms for cardiac repair. SIS-ECM is shown to induce a reparative phenotype in macrophages and promotes cardiac recruitment of proangiogenic neutrophils and monocytes.[24,33] Given the pericardial cavity's slow molecular turnover and direct communication with the heart, pericardial delivery of micronized SIS-ECM (mSIS-ECM) may provide a sustained release of ECM-bound molecules to modulate pericardial and myocardial inflammatory responses toward adaptive repair with recovery of tissue function.[34]

Herein, we perform a proof-of-concept study for the use of mSIS-ECM to promote cardiac repair after ischemic injury, using a pericardial space delivery approach. First, we validate the micronized form of SIS-ECM's bioinductivity and show a less fibrotic and proangiogenic fibroblast phenotype. Next, we demonstrate biomaterial-specific immunomodulation and identify an eosinophil-focused response within the pericardial space and myocardium of non-infarcted and infarcted mice. Finally, the biomaterial is shown to increase myocardial angiogenesis and restore cardiac tissue function in wild-type (WT) mice. The biomaterial-mediated benefits on angiogenesis and function are lost in eosinophil-knockout (KO) mice, uncovering a critical immune cell mechanism for the proposed therapy. For the first time, to our knowledge, we show that pericardial delivery of mSIS-ECM modulates fibroblast activity and recruits eosinophils to stimulate adaptive postinfarct cardiac repair.

METHODS

PREPARATION OF BIOMATERIALS. The biomaterial was a micronized form of acellular porcine intestinal submucosal extracellular matrix donated in kind by CorMatrix Cardiovascular Inc. The non-micronized source material has already received approval from the U.S. Food and Drug Administration (Cor PATCH, CorMatrix Cardiovascular Inc).[9] For in vitro 3T3 fibroblast studies, the material was prepared in Dulbecco's modified Eagle medium (DMEM) (Lonza) with 5% fetal bovine serum. For in vitro human cardiac fibroblast studies, the material was prepared in Iscove modified Dulbecco medium (Lonza) with 5% fetal bovine serum. For in vivo mouse studies involving pericardial injection, the material was prepared in normal saline (1.6 mg of mSIS-ECM in 40 μL of normal saline).

FIBROBLAST RESPONSE TO BIOMATERIAL. Mouse 3T3 cell line fibroblasts were used for in vitro studies. Because the pericardial injection strategy does not involve direct biomaterial implantation into or over the myocardium, the in vitro model focused on eluted components from the biomaterial. Biomaterial-conditioned media (CM) was first made by immersing 4.5 mg of mSIS-ECM in 700 μL of DMEM cell culture media with 5% fetal bovine serum for 24 hours; then, the solid micronized material was removed via centrifugation. The CM was added to 3-dimensional cultures of 400,000 mouse 3T3 cells in collagen gel in 24-well cell culture plates. Plates were incubated at 37 °C and 5% CO_2. The 3-dimensional cultures were exposed to the CM, released at 24 hours, and exposed to CM for a total of 48 hours. After treatment, a series of assays were performed to assess fibroblast modulation.

Images were obtained of the 24-well places that held the 3-dimensional cultures (iPhone 12 Pro Max, Apple). Gel contraction was quantified on Image J (National Institutes of Health). After images were taken, the CM was taken for multiplex analysis (Luminex, Eve Technologies). The gels were then fixed for 1 hour in 4% paraformaldehyde at room temperature and then stained overnight using 1:300 phalloidin and 1:300 Hoechst stain in phosphate-buffered saline (PBS) at 4 °C. The cells were then imaged under confocal microscopy for morphologic analysis. Morphology was assessed on Image J, with focus on cell area, number of projections, projection length, circularity, and roundness.

CHARACTERIZATION OF ELUTED FACTORS FROM mSIS-ECM BIOMATERIAL. CM was prepared as described. After a 24-hour elution period, the CM was analyzed via multiplex (Eve Technologies). Results were compared to unconditioned culture media (DMEM with 5% fetal bovine serum).

PARACRINE RESPONSE FROM HUMAN PERICARDIAL FLUID CELLS. Native human pericardial fluid was retrieved from 6 consenting patients undergoing nonemergent cardiac surgery. Pericardial fluid was collected during the surgery after the pericardium was opened and before the initiation of cardiopulmonary bypass. On gross examination, all samples were devoid of any blood. The cellular component of pericardial fluid was isolated via centrifugation (1,600 revolutions/min, 4 minutes, 4 °C). From each patient, 300,000 cells were allocated to the control and treatment groups. In a 6-well tissue culture plate, each patient's native pericardial fluid cells were exposed to 3 mL of cell culture media alone (Iscove modified Dulbecco medium with 5% fetal bovine serum) (control) or 3 mL media containing 5 mg of mSIS-ECM (treatment). Plates were incubated at 37 °C with 5% CO_2. After 24 hours, conditioned cell culture media was collected from each well and analyzed for levels of eotaxin using multiplex protein quantification.

ANIMALS. All in vivo experiments involved male WT mice (C57BL/6) or eosinophil-KO mice (Gata1 KO) (B6.129S1(C)-Gata1tm6Sho/LvtzJ) aged 8 to 12 weeks. Mice were purchased from The Jackson Laboratory and bred in house. Mice were housed at the University of Calgary under a specific pathogen-free, double-barrier unit. Mice were provided autoclaved

FIGURE 1   Pericardial Delivery of mSIS-ECM Preserves Postinfarct Cardiac Function and Improves Angiogenic Remodeling
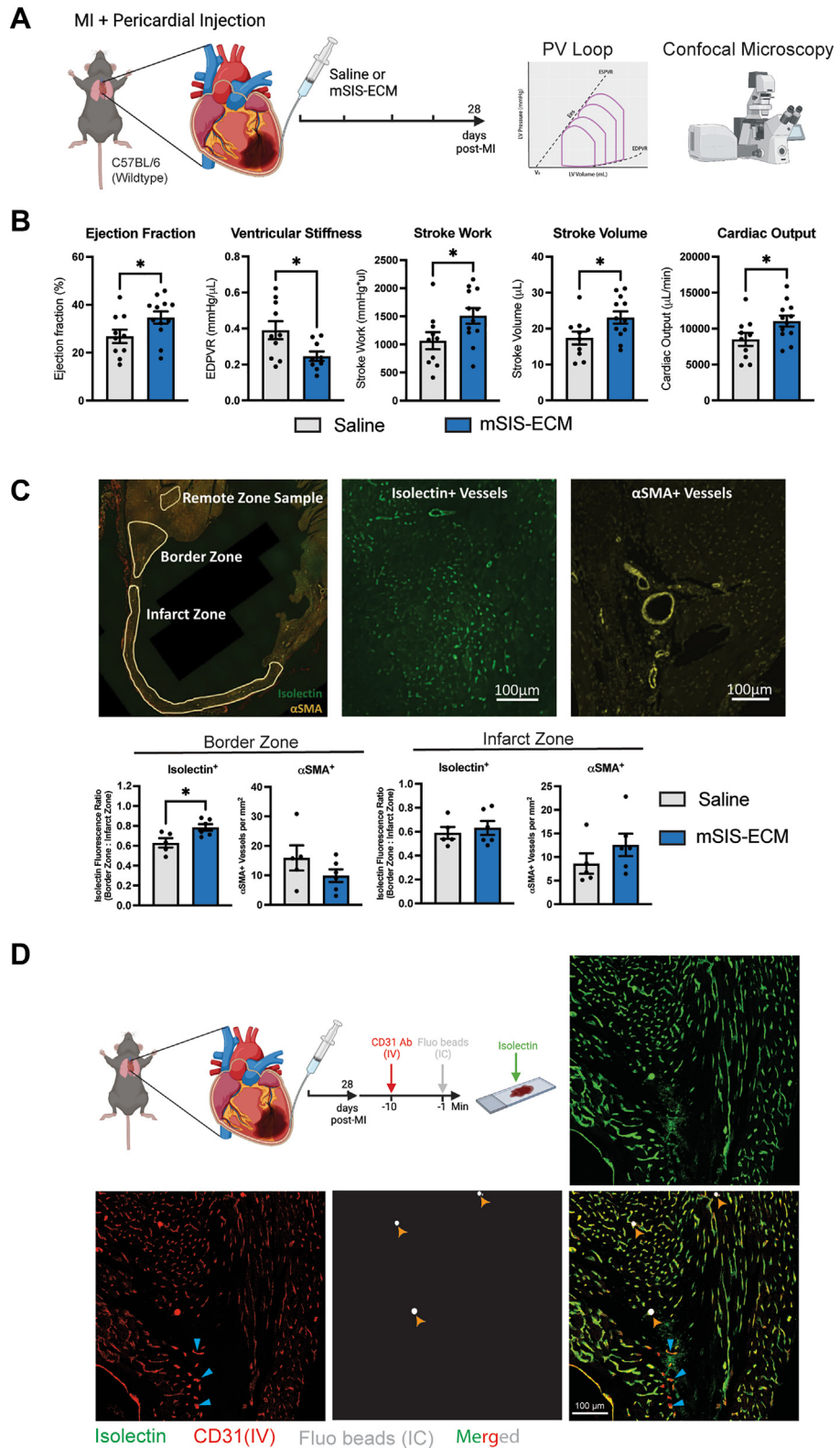
rodent feed and water. All protocols were in accordance with the University of Calgary Animal Care Committee and the Canadian Council on the Use of Laboratory Animals.

MOUSE NONINFARCT PERICARDIAL DELIVERY MODEL. Pericardial delivery of mSIS-ECM was first performed in mice without MI. Anesthetic induction and maintenance were performed using isoflurane gas in an oxygen carrier at 4% and 2%, respectively. Intubation was achieved by a 23-gauge (G) cannula. The ventilator (VentElite Small Animal Ventilator, Harvard Apparatus) was set to 110 breaths/min and a tidal volume of 250 µL. Left-sided thoracotomy was performed through the third interspace. Mice were either injected with a 40-µL suspension of mSIS-ECM in normal saline (treatment) or 40 µL of normal saline (control). Layered chest closure was then performed with 5-0 Vicryl (Ethicon), with gentle suction provided using a 24-G catheter to evacuate residual thoracic air. Animals were sacrificed at 3 days for multiplex analysis of pericardial fluid obtained by lavage with 100 µL PBS (Lonza) and at 7 days for flow cytometry of the pericardial fluid and myocardium.

MOUSE INTACT PERICARDIUM CORONARY LIGATION MYOCARDIAL INFARCT MODEL. In vivo studies used a murine intact pericardium infarct model. Surgical infarction was performed as described previously.[25,35] Anesthetic and ventilation strategies were as described for noninfarcted mice. Left-sided thoracotomy was performed through the third interspace. The anterior interventricular artery was then visualized through the translucent pericardium. No pericardiotomy was performed because an intact pericardium was needed for the biomaterial injection. Instead, a suture (8-0 Ethilon [Ethicon]) was placed through the pericardium, surrounding the proximal anterior interventricular artery, and back through the pericardium; infarction was induced by tying down the vessel. After infarction, mice were either injected with a 40-µL suspension of mSIS-ECM in normal

saline (treatment) or 40 µL of normal saline (control). Layered chest closure was then performed with 5-0 Vicryl (Ethicon), with gentle suction provided using a 24-G catheter to evacuate residual thoracic air. Animals were sacrificed for cardiac explantation at 7 days for flow cytometry and assessment of myocardial homogenates and at 28 days for resonant confocal microscopy and cardiac functional analysis.

MOUSE PERICARDIAL AND MYOCARDIAL FLOW CYTOMETRY. Methods have been previously reported.[24,25] Pericardial lavage was performed in mice using a single 100-µL injection of sterile saline and centrifuged at 1,500 revolutions/min for 5 minutes at 4 °C to obtain pericardial fluid immune cells. Mouse ventricular myocardium was explanted, minced, and suspended in a PBS solution containing collagenase XI (125 U/mL) (Sigma), collagenase I (450 U/mL) (Sigma), DNase I (60 U/mL) (Roche), and hyaluronidase (60 U/mL) (Sigma) for 1 hour at 37 °C on an orbital shaker; then, the sample was passed through a 70-µm strainer and centrifuged at 60g for 5 minutes at 4 °C. Supernatant was collected and passed through a 40-µm cell strainer for a single-cell suspension. For heart samples, residual red blood cells were lysed using Ammonium-Chloride-Potassium solution (ACK) (Invitrogen). The cardiac and pericardial cells were blocked using anti-mouse CD16/32 antibody (2.4G2 clone, BioXcell) along with the viability dye Ghost Dye Red 710 (TONBO Biosciences) for 20 to 30 minutes. Cells were then stained for 20 minutes with primary antibody cocktails. For intracellular staining of T-cell transcription factors and cardiac macrophage CD206, the Foxp3 staining kit (Thermo Fisher Scientific) and BD Cytofix/Cytoperm kit (BD Biosciences) were used, respectively. Appropriate isotype control antibodies were used to confirm positive intracellular signals. A BD FACS Canto flow cytometer was used, with analysis via FlowJo (Tree Star). In the heart, we identified neutrophils (CD11b$^+$Ly6G^{hi}Ly6C^{int}),

---

FIGURE 1 Continued

(A) Wild-type mice received experimental myocardial infarction through an intact pericardium, followed by pericardial delivery of mSIS-ECM or saline vehicle control and underwent cardiac function and histologic assessment at 28 days post-MI. **(B)** Quantification of PV loop assessment of ventricular stiffness, ejection fraction, stroke work, stroke volume, and cardiac output following MI with or without mSIS-ECM pericardial delivery (n = 10 for saline; n = 9-12 for mSIS-ECM group). Unpaired Student's *t*-test used for statistical analysis with *$P < 0.05$. **(C)** Visualization and quantification of isolectin$^+$ vessels and α-SMA$^+$ medium to large vessels in the border and infarct zones following MI with or without mSIS-ECM pericardial delivery (n = 5 for saline control; n = 6 for mSIS-ECM). Unpaired Student's *t*-test used for statistical analysis with *$P < 0.05$. **(D)** Representative visualization of colocalization of in vivo labeling of border zone vasculature by preinjection fluorescently conjugated CD31 antibody (red) and fluorescent beads (white) along with postprocessing isolectin staining (green). Representative of 4 independent experiments. Data are presented as mean ± SEM in each graph. Experimental scheme graphics were created with BioRender.com. Ab = antibody; EDPVR = end-diastolic pressure-volume relationship; IC = intracoronary; IV = intravenous; MI = myocardial infarction; mSIS-ECM = micronized porcine small intestinal submucosal extracellular matrix; PV = pressure-volume; SMA = smooth muscle actin.

FIGURE 2   Pericardial Delivery of mSIS-ECM Promotes Eosinophilic Inflammatory Response in the Pericardium Following MI
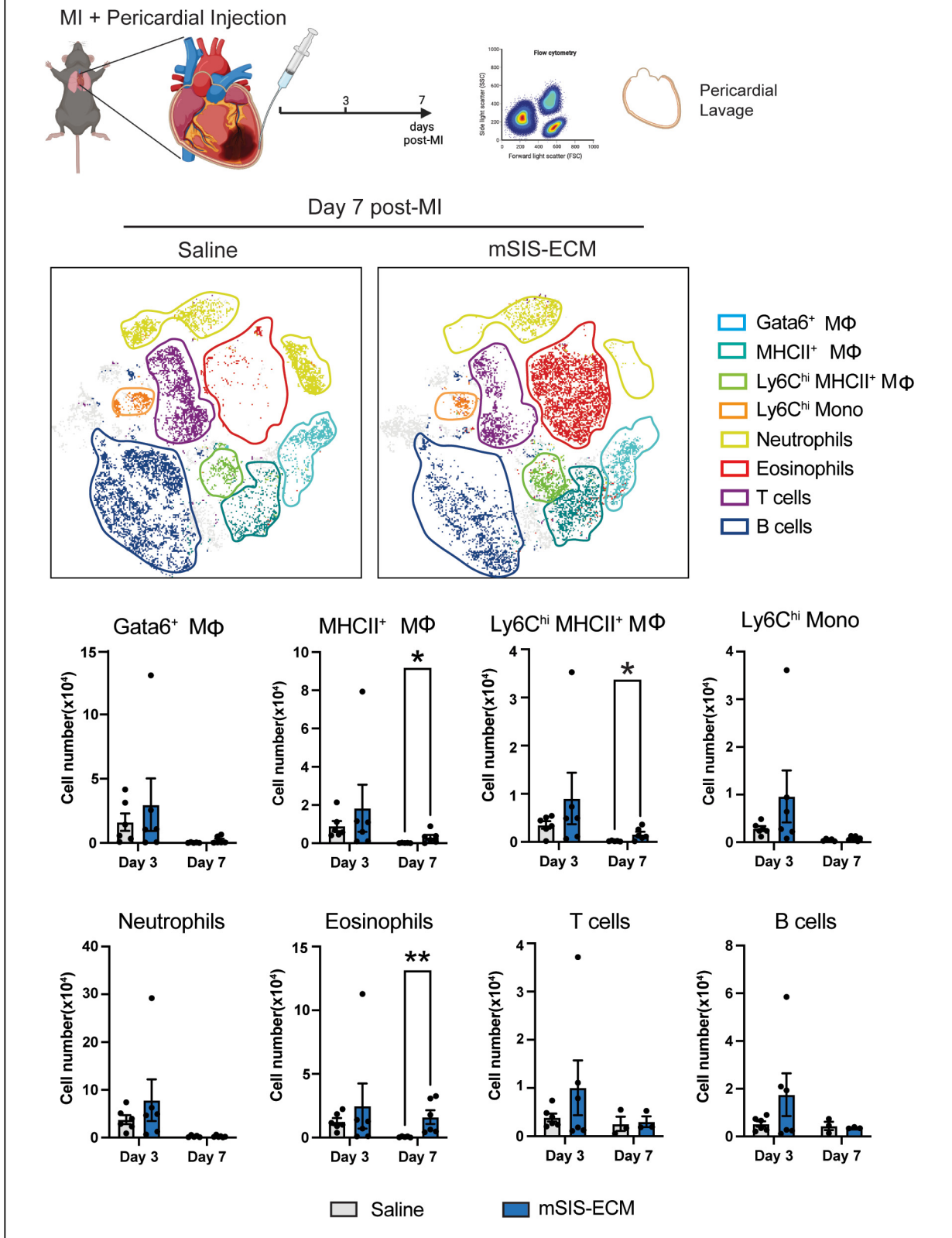
Representative flow cytometry data t-distributed stochastic neighbor embedding plots and quantification of the pericardial immune cell population in the pericardial lavage fluid at days 3 and 7 post-MI with either pericardial delivery of saline or mSIS-ECM (n = 6 for saline and mSIS-ECM groups at day 3, and n = 3-6 for saline and mSIS-ECM groups at day 7). Wilcoxon rank sum test was used for statistical analysis with *$P <$ 0.05 and **$P <$ 0.01. Data are presented as mean ± SEM in each graph. Experimental scheme graphics were created with BioRender.com. Abbreviations as in **Figure 1**.

FIGURE 3 Pericardial Delivery of mSIS-ECM Drives a Th2-Type Response in the Myocardium Following Ischemic Injury
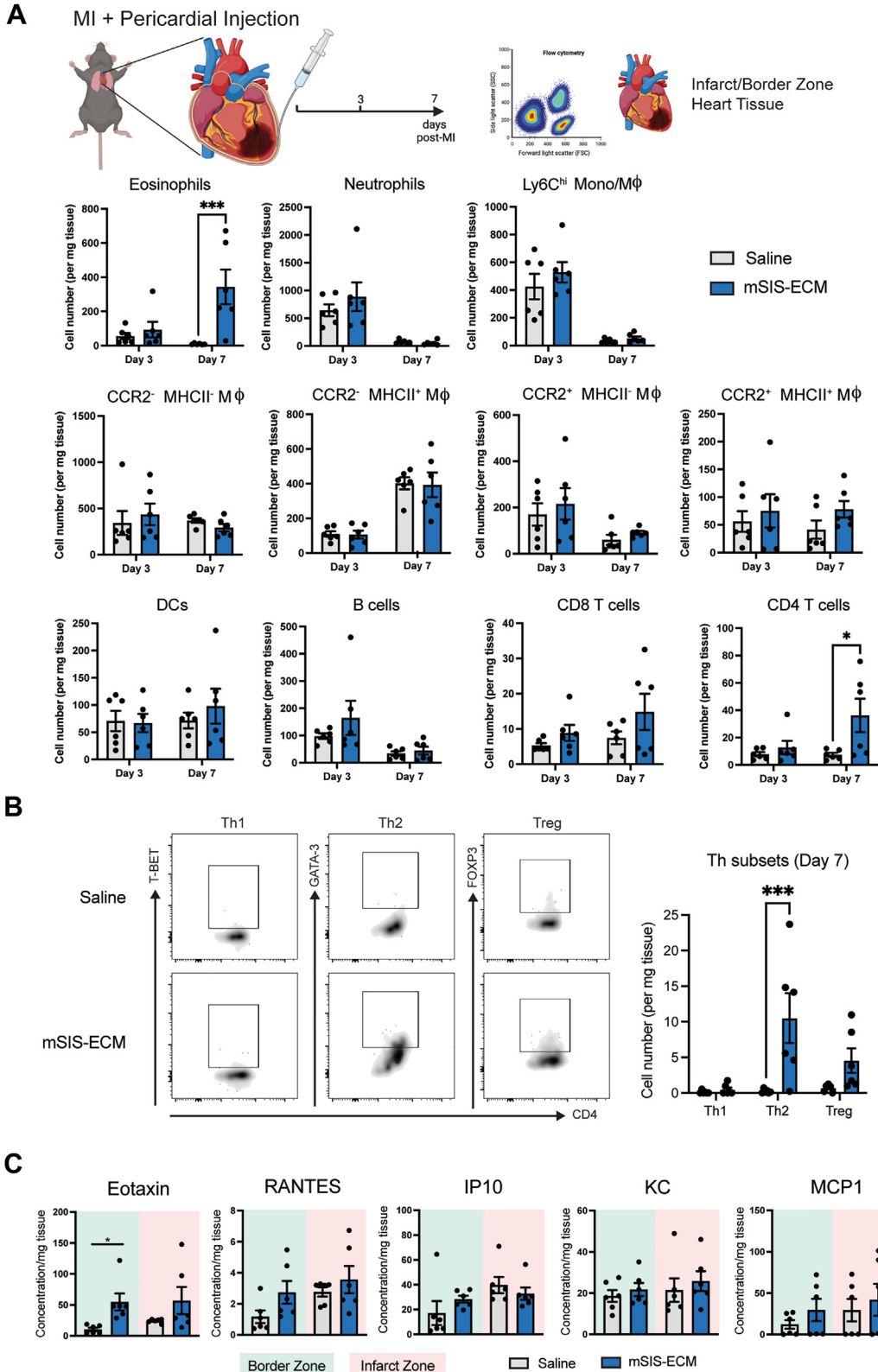
monocytes (CD11b$^+$Ly6G$^-$Ly6C^{hi}), macrophages (CD11b$^+$Ly6C^{lo}CD64$^+$MHCII$^{+/-}$CCR2$^{+/-}$, CD206$^{+/-}$), dendritic cells (CD11b$^+$CD64$^-$, Ly6G$^-$Ly6C$^-$MHCII$^+$), eosinophils (CD11b$^+$Siglec-F$^+$CD16$^-$SSc^{hi}), B cells (CD11b$^-$B220$^+$CD3$^-$), CD8 T cells (CD11b$^-$CD3$^+$CD8$^+$), Th1 CD4 T cells (CD11b$^-$CD3$^+$CD4$^+$T-bet$^+$), Th1 CD4 T cells (CD11b$^-$CD3$^+$CD4$^+$T-bet$^+$), T helper (Th) type 2 CD4 T cells (CD11b$^-$CD3$^+$CD4$^+$Gata3$^+$), and T-regulatory CD4 T cells (CD11b$^-$CD3$^+$CD4$^+$FOXP3$^+$). In the pericardial cavity, we identified Gata6$^+$ macrophages (CD11b$^+$CD102$^+$), neutrophils (CD11b$^+$Ly6G^{hi}), monocytes (CD11b$^+$CD102$^-$, MHCII$^-$, Ly6G$^-$Ly6C^{hi}), MHCII$^+$ macrophages (CD11b$^+$CD102$^-$Ly6C^{lo}MHCII$^+$), MHCII$^+$Ly6C$^+$ monocytes/macrophages (CD11b$^+$CD102$^-$Ly6C$^+$MHCII$^+$), eosinophils (CD11b$^+$Siglec-F$^+$CD16$^-$SSc^{hi}), B cells (CD11b$^-$B220$^+$CD3$^-$), and CD8 T cells (CD11b$^-$CD3$^+$).

MYOCARDIAL HOMOGENATE ANALYSIS. WT C57BL/6 mice underwent coronary ligation and pericardial injection with either mSIS-ECM suspension or saline as described earlier. After 7 days, the left ventricular myocardium was procured and separated into the infarct zone, border zone, and remote zone. Using a tissue homogenizer, each zone was homogenized in 500-μL serum-free DMEM cell culture media and centrifuged at 8,000 revolutions/min for 10 minutes. Growth factor and cytokine concentrations in the supernatant were then analyzed via multiplex. Concentrations were normalized for total protein using a Bradford assay.

IMMUNOHISTOCHEMISTRY AND RESONANT CONFOCAL MICROSCOPY. Specimens were prepared for staining by the core pathology laboratory of the Libin Cardiovascular Institute (University of Calgary). Staining and imaging methods have been described previously.[24] After fixing in 10% buffered formalin, specimens were embedded in paraffin and sectioned with a microtome onto slides. Then the specimens were deparaffinized and dehydrated using toluene and an alcohol series. Small vessels in the myocardium were highlighted with an isolectin stain. Autofluorescence of isolectin, podoplanin, and α-smooth muscle actin

(SMA) was reduced by immersing slides in 50 mmol/L ammonia in 70% ethanol for 60 minutes, followed by 5 minutes in 0.1% Sudan Black B in 70% ethanol. Slides were incubated for 60 minutes with 10 mmol/L citric acid in 0.05% Tween at pH 6.0 and 95 to 100 °C for antigen retrieval. After a 1-hour blocking period using 5% goat serum and 0.1% Triton X-100 in PBS, slides were stained using primary α-SMA (1:300 in 1% bovine serum albumin) in a 4 °C cold room overnight. Then we added secondary anti-mouse 555 (1:300), isolectin (1:60), and podoplanin (1:100) in 0.2-mmol/L calcium chloride solution for 2-hour incubation at room temperature (isolectin-conjugated Alexa Fluor 488 [Vector Laboratories], podoplanin allophycocyanin-conjugated antibody [Podoplanin Monoclonal Antibody, eFluor 660, Thermo Fisher Scientific], anti-mouse α-SMA [A-5228, Sigma]). Slide covers were mounted with Prolong Gold antifade reagent (P36930, Invitrogen). For studies determining cardiac capillary vessel perfusion, additional prelabeling steps were added. At 4 weeks post-MI, mice were first perfused intravenously with an AF647-conjugated anti-CD31 antibody 10 minutes before sacrifice, and then just before sacrifice received an intracardiac injection of fluorescent beads. Collected hearts were then fixed overnight in 4% paraformaldehyde, sequentially incubated in a sucrose solution before mounting in optimal cutting temperature compound, and sectioned on a cryotome onto slides. Isolectin staining and mounting were performed as described earlier. Imaging was performed with a Leica TCS SP8 resonant scanning confocal microscope and Leica LAS X software. Composite stitch images containing all of the infarcted region, border zones, and remote zone were completed for a full representation of the distinct areas. Total infarcted area and border zones combining multiple fields of view were analyzed on ImageJ using the Bio-Formats Plugin (https://www.openmicroscopy.org/bio-formats/). Small vessel vascular density was quantified with regional isolectin fluorescence. Larger α-SMA$^+$ blood vessels,

---

FIGURE 3   Continued

(A) Quantification of the pericardial immune cell population in the combined border and infarct zone tissue at days 3 and 7 post-MI with either pericardial delivery of saline or mSIS-ECM (n = 6 for saline and mSIS-ECM groups at day 3, and n = 6 for saline and mSIS-ECM groups at day 7). Wilcoxon rank sum test was used for statistical analysis with *$P < 0.05$ and ***$P < 0.001$. **(B)** Representative flow plots of CD4$^+$ T-cell transcription factor expression and quantification of Th1, Th2, and Treg subsets in the combined border and infarct zone tissue at day 7 post-MI with either pericardial delivery of saline or mSIS-ECM (n = 6 for the saline and mSIS-ECM groups). Wilcoxon rank sum test was used for statistical analysis with ***$P < 0.001$. **(C)** Quantification of chemokine content identified in border and infarct zone myocardial homogenates (n = 6/group). Unpaired Student's *t*-test was used for statistical analysis. *$P < 0.05$. Data are presented as mean ± SEM in each graph. Experimental scheme graphics were created with BioRender.com. DC = dendritic cell; KC = keratinocyte chemoattractant; Th = T helper; Treg = T regulatory; other abbreviations as in **Figure 1**.

FIGURE 4 Pericardial mSIS-ECM Alters Angiogenic and Inflammatory Protein Content in the Myocardial Border Zone
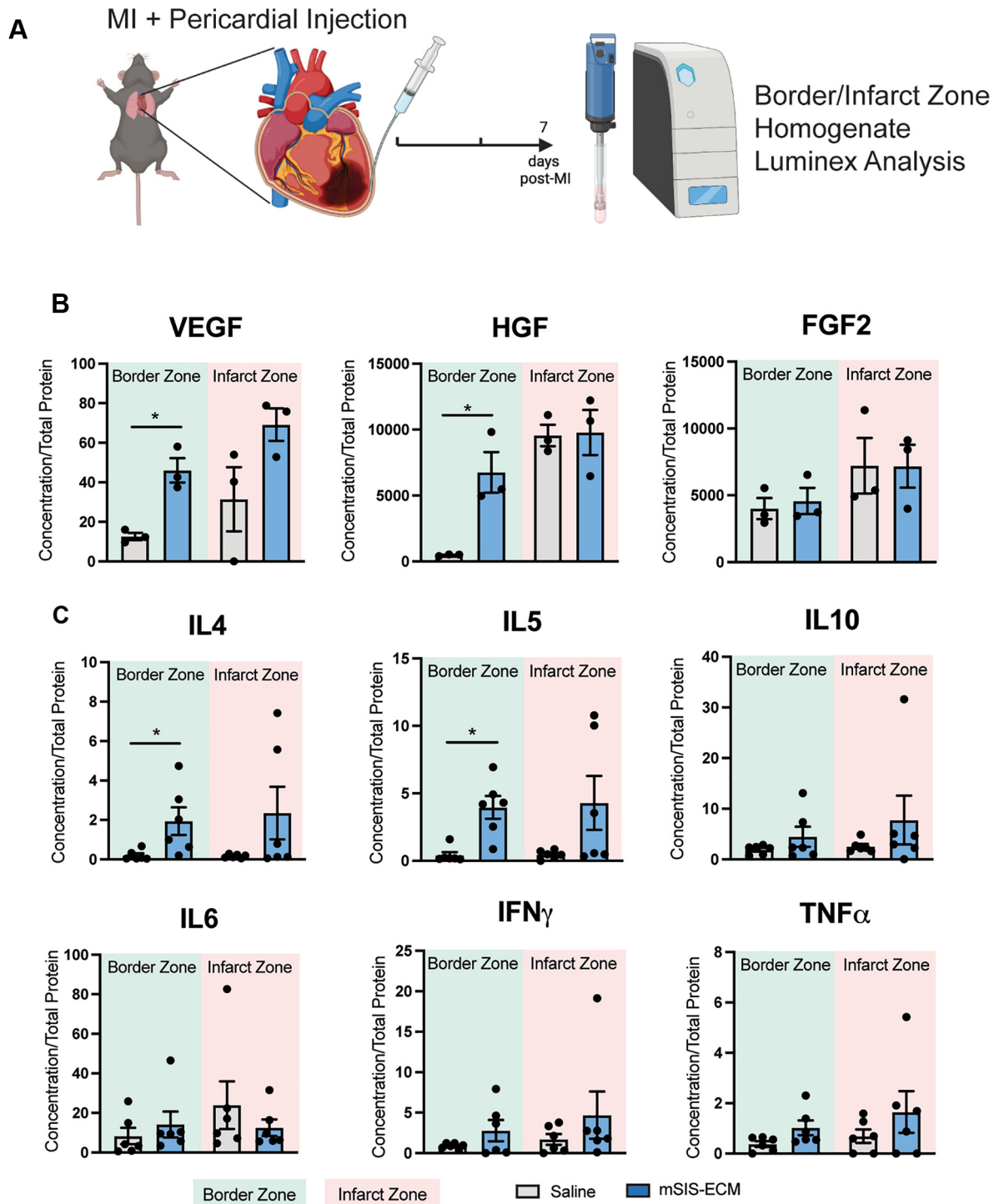
(A) In wild-type mice, experimental MI was induced, followed by pericardial delivery of mSIS-ECM or saline vehicle control, followed by cytokine evaluation on the border and infarct zone tissue lysates. **(B)** Quantification of angiogenic VEGF, HGF, and FGF-2 protein content identified in border and infarct zone myocardial homogenates (n = 3/group). **(C)** Quantification of anti-inflammatory and proinflammatory cytokine content identified in border and infarct zone myocardial homogenates (n = 6/group). Unpaired Student's *t*-test was used for statistical analysis. *$P < 0.05$. Data are presented as mean ± SEM in each graph. Experimental scheme graphics were created with BioRender.com. FGF = fibroblast growth factor; HGF = hepatocyte growth factor; IFN = interferon; IL = interleukin; MI = myocardial infarction; TNF = tumor necrosis factor; VEGF = vasculogenic endothelial growth factor.

which are also positive for isolectin, were counted and normalized to the total area.

CARDIAC FUNCTION ASSESSMENT. At 28 days post-infarct and treatment, invasive pressure-volume loops were used to assess cardiac function. Anesthetic induction and maintenance were performed with isoflurane at 4% and 2%, respectively. Mice were intubated and ventilated with a VentElite Small Animal Ventilator (Harvard Apparatus). The neck was shaved, cleaned, and incised to expose the right carotid artery, which was occluded distally, and a 1-F conductance catheter (Millar Instruments) was gently advanced into the left ventricle. After baseline measurements, abdominal occlusion of the vena cava was performed for parameters requiring multiple preloads. Finally, parallel conductance was obtained by jugular vein injection of hypertonic saline, and conductance was calibrated with blood. Animals were sacrificed, and hearts were explanted for other studies. LabChart (ADI Instruments) was used for pressure-volume loop analysis.

STATISTICAL ANALYSIS. Data are represented as mean ± SEM. Group comparisons were performed using Student's *t*-test or Wilcoxon rank sum test, dependent on data distribution. A *P* value of <0.05 was considered statistically significant. Analysis and graphical representation were performed via Graph-Pad Prism 8 software (GraphPad Software Inc), Bio-Render (BioRender), and PowerPoint (Microsoft).

RESULTS

VALIDATION OF BIOINDUCTIVITY: mSIS-ECM PROMOTES A LESS FIBROTIC, PROANGIOGENIC, AND PROINFLAMMATORY FIBROBLAST PHENOTYPE.

Fibroblast cultures validated mSIS-ECM's bioinductivity after micronization. We previously demonstrated a redirection of fibroblasts from a maladaptive profibrotic phenotype toward a proangiogenic phenotype when seeded directly on bioinductive SIS-ECM sheets. However, because mSIS-ECM is not fixed to the heart, an indirect model was developed and used to assess bioinductivity on adjacent cells. Mouse 3T3 fibroblasts seeded in collagen matrices were exposed to CM for 48 hours (Supplemental Figure 1A).[11,24]

Collagen gel contraction and matrix metalloproteinase (MMP)-2 production served as metrics of fibrotic activity.[12] Profibrotic transforming growth factor (TGF)-β increased gel contraction. The mSIS-ECM CM reduced gel contraction with and without TGF-β (Supplemental Figure 1B). On multiplex, mSIS-ECM reduced MMP2 release (Supplemental Figure 1C).

Given recent findings demonstrating that SIS-ECM up-regulates fibroblast angiogenic and inflammatory activity, multiplex also quantified the release of growth factors and inflammatory cytokines.[24] Consistent with proangiogenic signaling, the mSIS-ECM CM increased 3T3 fibroblast release of vascular endothelial growth factor (VEGF) and hepatocyte growth factor proteins, which was further potentiated by concomitant TGF-β addition (Supplemental Figure 1D). Exposure to mSIS-ECM CM increased fibroblast release of granulocyte colony-stimulating factor, interleukin (IL)-6, macrophage inflammatory protein (MIP)-2, and interferon gamma–induced protein (IP)-10 , showing a capacity for the biomaterial to modulate inflammatory responses (Supplemental Figure 1E).

PERICARDIAL INJECTION OF mSIS-ECM IMPROVES CARDIAC FUNCTION IN A MURINE INFARCT MODEL.

Following verification of in vitro bioactivity of mSIS-ECM, we next evaluated whether this would translate to protection following cardiac injury. MI was induced by suture ligation of the anterior interventricular artery through an intact unopened pericardium.[19,24] In the same procedure, mSIS-ECM suspended in normal saline was injected into the pericardial space (Figure 1A). This model allows preservation of the pericardial space for therapeutic delivery with retention of native pericardial fluid and immune cells. Pressure-volume loop and tissue remodeling assessments were performed 28 days after infarction and biomaterial injection.

mSIS-ECM reduced the end-diastolic pressure-volume relationship when compared to the control group, representing a decrease in ventricular stiffness and an increase in ventricular compliance (Figure 1B). Pericardial injection of the material also increased ejection fraction, stroke work, cardiac output, and stroke volume (Figure 1B, Supplemental Table 1). Overall, the material improved load-insensitive indexes of both systolic and diastolic cardiac function.

Myocardial resonant confocal microscopy was performed to investigate biomaterial-induced myocardial changes responsible for improved cardiac function at postinfarct day 28. Normalized isolectin mean fluorescence was used as a marker of small blood vessel density (Figure 1C), revealing that mSIS-ECM enhanced vascularity in the border zone relative to control animals (Figure 1C). In contrast, no differences were observed in the infarct zone. mSIS-ECM did not increase border zone counts of α-SMA⁺ medium- to large-sized blood vessels, which are also isolectin⁺, suggesting that this new vascularity was primarily composed of smaller capillary-like vessels

FIGURE 5 Pericardial Delivery of mSIS-ECM Does Not Preserve Postinfarct Cardiac Function in the Absence of Eosinophils

(A) Eosinophil-deficient (Gata1 KO) mice received experimental MI through an intact pericardium, followed by pericardial delivery of mSIS-ECM or saline vehicle control and underwent cardiac function and histologic assessment at 28 days post-MI. (B) Quantification of PV loop assessment of ventricular stiffness, ejection fraction, stroke work, stroke volume, and cardiac output following MI with or without mSIS-ECM pericardial delivery (n = 10 for saline, and n = 9 for the mSIS-ECM group). Unpaired Student's *t*-test was used for statistical analysis. (C) Quantification of isolectin$^+$ vessels and α-SMA$^+$ medium to large vessels in the border and infarct zones following MI with or without mSIS-ECM pericardial delivery (n = 5 for saline control, and n = 4-5 for mSIS-ECM). Unpaired Student's *t*-test was used for statistical analysis. Data are presented as mean ± SEM in each graph. Experimental scheme graphics were created with BioRender.com. KO = knockout; other abbreviations as in Figure 1.

(Figure 1C). To evaluate whether these isolectin$^+$ structures in the border zone were perfused, we delivered a fluorescently conjugated CD31 antibody intravenously and fluorescent beads in the left ventricle of the heart before sacrifice (Figure 1D). The majority of isolectin$^+$ structures were costained with the in vivo CD31 label, including vessels found within the infarcted tissue of the border zone (blue arrows). The presence of fluorescent beads (orange arrows) in these regions suggests active blood flow (perfusion) in the border zone vasculature. Some myocardial regions showed more diffuse isolectin staining without CD31 colabeling, likely identifying immature vessel structures.

PERICARDIAL mSIS-ECM PROMOTES AN EOSINOPHIL-FOCUSED PERICARDIAL AND MYOCARDIAL IMMUNE RESPONSE AFTER MI. The postinfarct inflammatory

response in the pericardium and injured heart is a key determinant of cardiac remodeling and influences the balance between adaptive angiogenic and maladaptive fibrotic tissue healing.[25,36] Using the intact pericardium mouse infarct model, mSIS-ECM induced shifts in the local immune response in the pericardium and neighboring myocardium. Immune cell profiles were evaluated at days 3 and 7 post-MI by flow cytometry (**Figures 2 and 3**). Flow cytometry gating strategies are shown in Supplemental Figure 2. In the pericardial space, the immune response was unchanged at day 3 post-MI with no differences between the saline and mSIS-ECM groups. However, mSIS-ECM contributed to a sustained immune response at day 7 post-MI with specific increases in both eosinophils and MHCII$^+$ macrophages (**Figure 2**). Of note, pro-reparative Gata6$^+$ macrophages, Ly6C^{lo} MHCII$^+$ macrophages, monocytes, neutrophils, and lymphoid populations were unchanged (**Figure 2**). Parallel flow cytometry of the neighboring infarcted myocardium (infarct and border zone) revealed a similar immune response. No differences between myeloid and lymphoid populations were noted at the early day 3 timepoint (**Figure 3A**). At day 7 post-MI, eosinophil counts were significantly increased in the infarcted tissue, mirroring the response in the pericardium (**Figure 3A**). In addition, increases in CD4$^+$ T cells were also confirmed at this timepoint. Transcription factor analysis of the CD4$^+$ T-cell population further revealed that this increase was predominantly caused by increases in Th2 populations (Gata3$^+$) (**Figure 3B**).

Chemokine assessment of the infarct heart tissue at day 7 post-MI revealed elevated levels of eotaxin, a key eosinophil chemokine, in the border zone in mSIS-ECM–treated mice relative to saline control (**Figure 3C**). No significant changes were observed in other chemokines in the border zone and no changes overall in the infarcted tissue. Collectively, these data show that mSIS-ECM sustains a localized eosinophilic response in the injured heart with stimulation of a Th2 response.

BIOMATERIAL-SPECIFIC IMMUNOMODULATION: mSIS-ECM PROMOTES AN EOSINOPHIL-MEDIATED PERICARDIAL AND MYOCARDIAL IMMUNE RESPONSE IN NONINFARCTED MICE. To test the direct ability of mSIS-ECM to stimulate this local inflammatory response, we repeated pericardial delivery of mSIS-ECM in the absence of ischemic injury (sham surgery) (Supplemental Figure 3A). The same eosinophilic response in both the pericardial cavity and heart were observed at day 7 post-injection (Supplemental Figures 3B and 3C). This response was further complemented by increases in Ly6C^{hi}MHCII$^+$ macrophages (Supplemental

Figure 3B) and dendritic cells (Supplemental Figure 3C) in the pericardial cavity and heart, respectively. Other myeloid populations remained unchanged in both compartments (Supplemental Figure 3B and 3C).

Levels of eotaxin, a key eosinophil chemoattractant, were evaluated at 3 days post–mSIS-ECM delivery before their recruitment in the noninfarct mouse model to assess the local regulation of eosinophil recruitment to the pericardial space At this timepoint, eotaxin analysis showed a trend for increased eotaxin concentrations in the pericardial fluid of the mSIS-ECM treatment group relative to the control group (Supplemental Figure 3D). We explored the potential cellular sources of this eotaxin. We first tested fibroblasts, which are key sources of chemokines in the heart and are stimulated by mSIS-ECM (Supplemental Figure 1). Despite the induction of many other inflammatory mediators, fibroblast incubation with mSIS-ECM CM did not elicit a change in eotaxin secretion (data not shown). To evaluate a more local source within the pericardial space, human pericardial fluid cells were isolated from patients undergoing cardiac surgery and exposed to either mSIS-ECM suspension or control cell culture media. After 24 hours, mSIS-ECM increased the production of eotaxin in human pericardial fluid cells, demonstrating that these cells serve as mediators of the eosinophilic response (Supplemental Figure 3E). These data support that mSIS-ECM can directly initiate the eosinophilic response described through local production of eotaxin by resident pericardial immune cells. This may represent a mechanism of entry for eosinophils into the pericardial space and subsequent migration into the myocardium.

PERICARDIAL mSIS-ECM INCREASES MYOCARDIAL CONTENT OF EOSINOPHIL-RELATED FACTORS AND ANGIOGENIC PROTEINS. To determine how these mSIS-ECM–induced immune cell changes coincided with the local molecular profiles in the infarcted heart, myocardial cytokine and growth factor production were evaluated in the infarct and border zone by multiplex protein analysis (**Figure 4A**). Inflammatory and angiogenic proteins were quantified at day 7 as post-MI angiogenesis peaks within the first week, and SIS-ECM prolongs inflammation to this timepoint.[24,37] The border zone was of key interest because it transitions between the infarct and remote zones, and its dynamic remodeling may be most influenced by mSIS-ECM.

Regarding angiogenic protein content at day 7 post-MI, border zone homogenates in the mSIS-ECM group contained higher concentrations of angiogenic

VEGF and hepatocyte growth factor but not fibroblast growth factor 2 (FGF-2) (**Figure 4B**). There were no changes observed in the infarct zone. Given that eosinophils have been shown to produce VEGF and potentiate angiogenesis, these cells may contribute to the increase in angiogenic factor content.[38,39] Myocardial border zone homogenates in the mSIS-ECM group also showed increased concentrations of IL-4 and IL-5 (**Figure 4C**), key eosinophil mediators,[26,40,39] further emphasizing an eosinophil-specific response. This response appeared to be specific because other mediators, including both anti-inflammatory (IL-10) and proinflammatory (IL-6, interferon gamma, tumor necrosis factor α), were unchanged after pericardial delivery of mSIS-ECM following MI. Eosinophils were previously shown to promote more optimal healing via early macrophage polarization defined by a CD206$^+$ reparative phenotype in an IL-4-dependent manner.[26] Analysis of CD206$^+$ cardiac macrophage numbers in the infarcted myocardium at both days 3 and 7 revealed no differences between saline- and mSIS-ECM-treated animals (Supplemental Figure 4). This shows that mSIS-ECM contributes to local changes in cytokines and growth that can dictate the healing response in the heart.

PERICARDIAL mSIS-ECM ENHANCES MYOCARDIAL NEOVASCULARIZATION BY LEVERAGING AN EOSINOPHIL-BASED RESPONSE.

To determine whether eosinophils are required for the beneficial effects promoted by mSIS-ECM pericardial delivery, we performed cardiac function and tissue remodeling assessment at postinfarct day 28 using Gata1 KO (eosinophil KO) (**Figure 5A**). Genetic eosinophil depletion eliminated the cardioprotective effects of mSIS-ECM documented in WT animals (**Figure 5B**), with no observed benefit to ventricular stiffness, ejection fraction, stroke work, stroke volume, or cardiac output (**Figure 5B**). Additionally, maximum dP/dt, minimum dP/dt, and end-systolic pressure worsened in eosinophil-deficient animals with the addition of mSIS-ECM compared to control (Supplemental Table 2).

Imaging was also performed for mice to examine the role of eosinophils in biomaterial-mediated angiogenic changes. Resonant confocal myocardial imaging identified that eosinophil depletion prevented the biomaterial-mediated increase in border zone small vessel density seen in WT mice because there was no difference in normalized isolectin mean fluorescence between groups (**Figure 5C**, and there were no changes in α-SMA$^+$ vessels. There were also no differences in the infarct zone (**Figure 5C**). These data emphasize, for the first time to our knowledge, the critical role of eosinophils in biomaterial-mediated cardiac angiogenesis and repair.

DISCUSSION

Acellular matrix biomaterials are valuable reservoirs of bioinductive components that can potentially bridge a longstanding therapeutic gap for IHD by redirecting cellular responses to promote adaptive healing. Building on previous work whereby biomaterials are administered via epicardial implantation or myocardial injection for postinfarct cardiac healing, our proof-of-concept study leverages a recently developed intact pericardium MI model to evaluate the pericardial space as a unique anatomic niche for cardiac repair and promising window for the delivery of novel immunomodulatory therapeutics.[11,12,19,24,25,28,34,35] Herein, we confirm mSIS-ECM's bioinductivity, identify an eosinophil-focused pericardial and myocardial response to the material itself, and then demonstrate that targeted pericardial biomaterial delivery after MI recruits pro-reparative eosinophil immune cells to promote myocardial neovascularization and preserve cardiac function.

Inflammatory responses to biomaterials are often considered maladaptive, and, as such, efforts are made to dampen these efforts. However, targeted immune stimulation in the heart context may actually benefit cardiac repair. Recent data show that improved cardiac function previously associated with stem cell therapy is linked to a monocytic immune response that can be mimicked using a generic inflammatory stimulus.[41] In addition, our recent work has shown that proangiogenic neutrophils and monocytes are recruited to the heart in response to epicardial implantation of SIS-ECM sheets.[24] Despite using the same base SIS-ECM biomaterial, delivery into the pericardial space and interaction with the local pericardial immune cells triggered a different inflammatory and immune response in the heart. This highlights the importance of the local in vivo environment in dictating the level and nature of response to these biomaterials. We show here that pericardial immune cells can contribute to this immunomodulation through the production of eotaxin to recruit eosinophils. Recent studies demonstrate that eosinophils optimize postinfarct cardiac remodeling, in part through their release of pro-reparative IL-4 that can shift the local inflammatory environment and promote pro-reparative macrophage polarization.[26,42] Importantly, these previous studies used eosinophil-deficient mice to demonstrate these effects in mice on a BALB/C background. This genetic

background in mice is noted to have a Th2-skewed immune response, thus favoring the involvement of eosinophils in the response. To stay consistent with our previous mouse work with the intact pericardium model and SIS-ECM work, the current study used mice on the C57BL/6 background that favor a Th1-type response and are associated with delayed repair mechanisms post-MI in mice.[43] Despite being on this genetic background, we show that mSIS-ECM itself induces an eosinophil-based Th2 inflammatory response, which can enhance angiogenesis and preserve cardiac function. This work in the heart mirrors similar work completed in the eye, where similar eosinophil and IL-4 signaling are involved in the benefits of bladder-derived ECM application for improving corneal wound healing.[44] This likely supports common mechanisms in ECM biomaterial-mediated modulation of host tissue immune responses.

Though often regarded as a passive inert barrier, the pericardium is a highly dynamic microenvironment with unique immune properties that can be leveraged by targeted therapeutics for cardiac healing.[25,26] The current study builds on previous work that has explored the delivery of drugs,[45-47] growth factors,[48-50] and biomaterials[52,51] to influence the neighboring cardiac environment. The use of biomaterials in this context has been previously limited to their role as a delivery scaffold for loading cells, cellular components, and viruses for potential gene therapy. Ladage et al[51] demonstrated that mesenchymal stem cells or live virus loaded on gel foam particles could effectively be delivered to the infarcted myocardium in pigs. Recently, Zhu et al[52] highlighted the use of stem cell-loaded decellularized ECM and exosome-based therapies via pericardial delivery to achieve repair. Interestingly, they found that the addition of stem cells on the decellularized ECM had a more profound effect on cardiac function than decellularized ECM alone when compared to an MI-only group. In contrast, the current study shows that a decellularized ECM, mSIS-ECM, alone can enhance the repair mechanisms in the injured heart. Differences in cardiac function post-MI between the mSIS-ECM and decellularized cardiac ECM used by Zhu et al may simply reflect differences in growth factor and/or nuclear material content between the 2 biomaterials. This also highlights the need for further investigation to streamline the effector molecules that regulate these beneficial effects. Although stem cell therapies are being investigated for postinfarct cardiac repair, results remain mixed because of issues with cell viability and engraftment, variable results, and unclear mechanisms.[41,53-56] Being devoid of viable cells, mSIS-ECM does not face viability- and engraftment-based barriers. Furthermore, mSIS-ECM is also derived from a commercially available biomaterial (CorMatrix Cor PATCH), which received approval from the U.S. Food and Drug Administration for postinfarct cardiac repair and could mitigate key barriers to effective clinical translation.[9] In addition, the SIS-ECM platform can potentially be modified with additional growth factors to optimize the therapy.[57]

Pericardial biomaterial delivery has clinical implications that can enhance how adjunct cardiovascular therapies are administered post-MI. Previous work with epicardial implantation of non-micronized SIS-ECM sheets is feasible only when a patient requires coronary artery bypass surgery, because this biomaterial approach requires an open-chest exposure for access to the surface epicardium of the injured heart.[12,19] However, pericardial delivery can be delivered in a less invasive format, potentially through a percutaneous procedure or thorascopic LARIAT-like approach.[52,58] A less invasive injectable strategy can widen the eligible patient population to those with IHD who do not require surgical intervention because this procedure can be performed in catheterization suites as an adjunct to angioplasty/stent procedures that open culprit vessel lesions. In addition, minimally invasive and less traumatic approaches provide cardiac care teams with the versatility to intervene earlier after MI to enhance adaptive angiogenic healing to provide multiple scheduled doses.

STUDY LIMITATIONS. In line with the potential application of an acute pericardial therapy, mSIS-ECM in this study was delivered immediately following ischemic injury. To further broaden clinical applicability, additional time course delivery testing is needed to better define the therapeutic window for this pericardial targeting. Additionally, study in older and diabetic mouse models may be more relevant to the target clinical population for this biomaterial therapy because these models may have impaired immune mechanisms that are potentially less likely to develop a proangiogenic phenotype. As a further step toward clinical translation, large animal studies will help with developing less invasive or percutaneous administration techniques and dose determination for the clinical setting.[52,58]

CONCLUSIONS

For the first time, we show that mSIS-ECM maintains its bioinductivity and that pericardial delivery of mSIS-ECM drives the recruitment of reparative immune cells to enhance myocardial angiogenesis and preserve cardiac function. These data highlight the key physical and immunologic properties of the pericardial cavity that make it promising for targeted biomaterial therapies. A versatile, less traumatic administration strategy may widen the eligible patient population for biomaterial therapies and provide an opportunity to intervene early after MI, potentially with multiple scheduled doses. Large animal models will be required for technique development as a bridge to clinical study.

FUNDING SUPPORT AND AUTHOR DISCLOSURES

ADDRESS FOR CORRESPONDENCE: Dr Paul W.M. Fedak, Heath Research and Innovation Centre, GC70 Foothills Campus, University of Calgary, 3230 Hospital Drive NW, Calgary, Alberta T2N 4N1, Canada. E-mail: paul.fedak@gmail.com.

PERSPECTIVES

COMPETENCY IN MEDICAL KNOWLEDGE: Micronized extracellular matrix biomaterials can augment postinfarct inflammation to mount an eosinophil-focused immune response in the pericardial space and myocardium. Pericardial delivery of a micronized ECM biomaterial increases angiogenic myocardial signaling and ultimately preserves postinfarct cardiac function.

TRANSLATIONAL OUTLOOK: This proof-of-concept study demonstrates a therapeutic signal for pericardial delivery of ECM biomaterials and identifies the eosinophil as a leverageable target for postinfarct cardiac repair. Future evaluation in large animal models is needed for clinical translation. A targeted pericardial delivery approach may facilitate less invasive strategies to administer biomaterial cardiac therapies and enable multiple scheduled doses for nonsurgical patients with ischemic heart disease.

REFERENCES

1. Virani SS, Alonso A, Aparicio HJ, et al. Heart disease and stroke statistics—2021 update: a report from the American Heart Association. *Circulation*. 2021;143(8):e254–e743.

2. Sueta CA. The life cycle of the heart failure patient. *Curr Cardiol Rev*. 2015;11(1):2–3. https://doi.org/10.2174/1573403x1101141106114520

3. Taylor DO, Stehlik J, Edwards LB, et al. Registry of the International Society for Heart and Lung Transplantation: twenty-sixth official adult heart transplant report—2009. *J Heart Lung Transplant*. 2009;28(10):1007–1022.

4. Neumann FJ, Sousa-Uva M, Ahlsson A, et al. 2018 ESC/EACTS guidelines on myocardial revascularization. *Eur Heart J*. 2019;40(2):87–165.

5. Teo KK, Cohen E, Buller C, et al. Canadian Cardiovascular Society/Canadian Association of Interventional Cardiology/Canadian Society of Cardiac Surgery position statement on revascularization multivessel coronary artery disease. *Can J Cardiol*. 2014;30(12):1482–1491.

6. Vasanthan V, Fatehi Hassanabad A, Pattar S, Niklewski P, Wagner K, Fedak PWM. Promoting cardiac regeneration and repair using acellular biomaterials. *Front Bioeng Biotechnol*. 2020;8:291. https://doi.org/10.3389/fbioe.2020.00291

7. Pattar SS, Fatehi Hassanabad A, Fedak PWM. Application of bioengineered materials in the surgical management of heart failure. *Front*

Cardiovasc Med. 2019;6:123. https://doi.org/10.3389/fcvm.2019.00123

8. Bannenberg G, Serhan CN. Specialized pro-resolving lipid mediators in the inflammatory response: an update. *Biochim Biophys Acta*. 2010;1801(12):1260–1273.

9. Vasanthan V, Biglioli M, Hassanabad AF, Dundas J, Matheny RG, Fedak PW. CorMatrix CorTM PATCH for epicardial infarct repair. *Future Cardiol*. 2021;17(8):1297–1305.

10. Pattar SS, Fatehi Hassanabad A, Fedak PWM. Acellular extracellular matrix bioscaffolds for cardiac repair and regeneration. *Front Cell Dev Biol*. 2019;7:63. https://doi.org/10.3389/fcell.2019.00063

11. Mewhort HEM, Svystonyuk DA, Turnbull JD, et al. Bioactive extracellular matrix scaffold promotes adaptive cardiac remodeling and repair. *J Am Coll Cardiol Basic Trans Science*. 2017;2(4):450–464.

12. Svystonyuk DA, Mewhort HEM, Hassanabad AF, et al. Acellular bioscaffolds redirect cardiac fibroblasts and promote functional tissue repair in rodents and humans with myocardial injury. *Sci Rep*. 2020;10(1):9459. https://doi.org/10.1038/s41598-020-66327-9

13. Fedak PWM, Verma S, Weisel RD, Li RK. Cardiac remodeling and failure: from molecules to man (part II). *Cardiovasc Pathol*. 2005;14(2):49–60.

14. Swynghedauw B. Molecular mechanisms of myocardial remodeling. *Physiol Rev*. 1999;79(1):215–262.

15. Gallagher GL, Jackson CJ, Hunyor SN. Myocardial extracellular matrix remodeling in ischemic heart failure. *Front Biosci*. 2007;12:1410–1419.

16. Davis J, Molkentin JD. Myofibroblasts: trust your heart and let fate decide. *J Mol Cell Cardiol*. 2014;70:9–18.

17. Brown RD, Ambler SK, Mitchell MD, Long CS. The cardiac fibroblast: therapeutic target in myocardial remodeling and failure. *Annu Rev Pharmacol Toxicol*. 2005;45:657–687.

18. Travers JG, Kamal FA, Robbins J, Yutzey KE, Blaxall BC. Cardiac fibrosis: the fibroblast awakens. *Circ Res*. 2016;118(6):1021–1040.

19. Mewhort HEM, Turnbull JD, Satriano A, et al. Epicardial infarct repair with bioinductive extracellular matrix promotes vasculogenesis and myocardial recovery. *J Heart Lung Transplant*. 2016;35(5):661–670.

20. Fedak PWM, Verma S, Weisel RD, Skrtic M, Li RK. Cardiac remodeling and failure: from molecules to man (part III). *Cardiovasc Pathol*. 2005;14(3):109–119.

21. Fedak PWM, Verma S, Weisel RD, Li RK. Cardiac remodeling and failure: from molecules to man (part I). *Cardiovasc Pathol*. 2005;14(1):1–11.

22. Saparov A, Ogay V, Nurgozhin T, et al. Role of the immune system in cardiac tissue damage and repair following myocardial infarction. *Inflamm Res*. 2017;66(9):739–751.

23. Massena S, Christoffersson G, Vågesjö E, et al. Identification and characterization of VEGF-A-responsive neutrophils expressing CD49d, VEGFR1, and CXCR4 in mice and humans. *Blood*. 2015;126(17):2016–2026.

24. Vasanthan V, Shim HB, Teng G, et al. Acellular biomaterial modulates myocardial inflammation and promotes endogenous mechanisms of post-infarct cardiac repair. *J Thorac Cardiovasc Surg*. 2023;165(3):e122–e140.

25. Deniset JF, Belke D, Lee WY, et al. Gata6(+) pericardial cavity macrophages relocate to the injured heart and prevent cardiac fibrosis. *Immunity*. 2019;51(1):131–140.

26. Toor IS, Rückerl D, Mair I, et al. Eosinophil deficiency promotes aberrant repair and adverse remodeling following acute myocardial infarction. *J Am Coll Cardiol Basic Trans Science*. 2020;5(7):665–681.

27. Spang MT, Christman KL. Extracellular matrix hydrogel therapies: In vivo applications and development. *Acta Biomater*. 2018;68:1–14.

28. Traverse JH, Henry TD, Dib N, et al. First-in-man study of a cardiac extracellular matrix hydrogel in early and late myocardial infarction patients. *J Am Coll Cardiol Basic Trans Science*. 2019;4(6):659–669.

29. Christman KL, Lee RJ. Biomaterials for the treatment of myocardial infarction. *J Am Coll Cardiol*. 2006;48(5):907–913.

30. Unger EF, Goncalves L, Epstein SE, et al. Effects of a single intracoronary injection of basic fibroblast growth factor in stable angina pectoris. *Am J Cardiol*. 2000;85(12):1414–1419.

31. Henry TD, Rocha-Singh K, Isner JM, et al. Intracoronary administration of recombinant human vascular endothelial growth factor to patients with coronary artery disease. *Am Heart J*. 2001;142(5):872–880.

32. Ali FH, Fedak PWM, Deniset JF. Acute ischemia alters human pericardial fluid immune cell composition. *J Am Coll Cardiol Basic Trans Science*. 2021;6(9-10):765–767.

33. Huleihel L, Dziki JL, Bartolacci JG, et al. Macrophage phenotype in response to ECM bio-scaffolds. *Semin Immunol*. 2017;29:2–13.

34. Trindade F, Vitorino R, Leite-Moreira A, Falcão-Pires I. Pericardial fluid: an underrated molecular library of heart conditions and a potential vehicle for cardiac therapy. *Basic Res Cardiol*. 2019;114(2):10. https://doi.org/10.1007/s00395-019-0716-3

35. Fatehi Hassanabad A, Belke DD, Turnbull J, et al. An intact pericardium ischemic rodent model. *J Vis Exp*. 2021;14(1):1–11. https://doi.org/10.3791/62720

36. Prabhu SD, Frangogiannis NG. The biological basis for cardiac repair after myocardial infarction: from inflammation to fibrosis. *Circ Res*. 2016;119(1):91–112.

37. Zhao T, Zhao W, Chen Y, Ahokas RA, Sun Y. Vascular endothelial growth factor (VEGF)-A: role on cardiac angiogenesis following myocardial infarction. *Microvasc Res*. 2010;80(2):188–194.

38. Puxeddu I, Alian A, Piliponsky AM, Ribatti D, Panet A, Levi-Schaffer F. Human peripheral blood eosinophils induce angiogenesis. *Int J Biochem Cell Biol*. 2005;37(3):628–636.

39. Davoine F, Lacy P. Eosinophil cytokines, chemokines, and growth factors: emerging roles in immunity. *Front Immunol*. 2014;5:570. https://doi.org/10.3389/fimmu.2014.00570

40. Nakajima T, Yamada H, Iikura M, et al. Intracellular localization and release of eotaxin from normal eosinophils. *FEBS Lett*. 1998;434(3):226–230.

41. Vagnozzi RJ, Maillet M, Sargent MA, et al. An acute immune response underlies the benefit of cardiac stem cell therapy. *Nature*. 2020;577(7790):405–409.

42. Shintani Y, Ito T, Fields L, et al. IL-4 as a repurposed biological drug for myocardial infarction through augmentation of reparative cardiac macrophages: proof-of-concept data in mice. *Sci Rep*. 2017;7(1):6877. https://doi.org/10.1038/s41598-017-07328-z

43. Toor IS, Rückerl D, Mair I, Thomson A, et al. Enhanced monocyte recruitment and delayed alternative macrophage polarization accompanies impaired repair following myocardial infarction in C57BL/6 compared to BALB/c mice. *Clin Exp Immunol*. 2019;198:83–93.

44. Wang X, Chung L, Hooks J, et al. Type 2 immunity induced by bladder extracellular matrix enhances corneal wound healing. *Sci Adv*. 2021;7:eabe2635. https://doi.org/10.1126/sciadv.abe2635

45. Tio RA, Grandjean JG, Suurmeijer AJH, van Gilst WH, van Veldhuisen DJ, van Boven AJ. Thoracoscopic monitoring for pericardial application of local drug or gene therapy. *Int J Cardiol*. 2002;82:117–121.

46. Xiao YF, Sigg DC, Ujhelyi MR, Wilhelm JJ, Richardson ES, Iaizzo PA. Pericardial delivery of omega-3 fatty acid: a novel approach to reducing myocardial infarct sizes and arrhythmias. *Am J Physiol Heart Circ Physiol*. 2008;294:H2212–H2218.

47. Moreno R, Waxman S, Rowe K, Verrier RL. Intrapericardial beta-adrenergic blockade with esmolol exerts a potent antitachycardic effect without depressing contractility. *J Cardiovasc Pharmacol*. 2000;36:722–727.

48. Uchida Y, Yanagisawa-Miwa A, Nakamura F, Yamada K, Tomaru T, Kimura K, et al. Angiogenic therapy of acute myocardial infarction by intrapericardial injection of basic fibroblast growth factor and heparin sulfate: an experimental study. *Am Heart J*. 1995;130(6):1182–1188.

49. Landau C, Jacobs AK, Haudenschild CC. Intrapericardial basic fibroblast growth factor induces myocardial angiogenesis in a rabbit model of chronic ischemia. *Am Heart J*. 1995;129(5):924–931.

50. Laham RJ, Rezaee M, Post M, et al. Intrapericardial delivery of fibroblast growth factor-2 induces neovascularization in a porcine model of chronic myocardial ischemia. *J Pharmacol Exp Ther*. 2000;292(2):795–802.

51. Ladage D, Turnbull IC, Ishikawa K, et al. Delivery of gelfoam-enabled cells and vectors into the pericardial space using a percutaneous approach in a porcine model. *Gene Ther*. 2011;18:979–985.

52. Zhu D, Li Z, Huang K, Caranasos TG, Rossi JS, Cheng K. Minimally invasive delivery of therapeutic agents by hydrogel injection into the pericardial cavity for cardiac repair. *Nat Commun*. 2021;12(1):1412. https://doi.org/10.1038/s41467-021-21682-7

53. Kaiser J. Suspect science leads to pause in stem cell trial. *Science*. 2018;362(6414):513. https://doi.org/10.1126/science.362.6414.513

54. Lancaster JJ, Sanchez P, Repetti GG, et al. Human induced pluripotent stem cell-derived cardiomyocyte patch in rats with heart failure. *Ann Thorac Surg*. 2019;108(4):1169-1177.

55. Huang K, Ozpinar EW, Su T, et al. An off-the-shelf artificial cardiac patch improves cardiac repair after myocardial infarction in rats and pigs. *Sci Transl Med*. 2020;12(538):eaat9683. https://doi.org/10.1126/scitranslmed.aat9683

56. Hata H, Bär A, Dorfman S, et al. Engineering a novel three-dimensional contractile myocardial patch with cell sheets and decellularised matrix. *Eur J Cardiothorac Surg*. 2010;38(4):450–455.

57. Park DSJ, Mewhort HEM, Teng G, et al. Heparin augmentation enhances bioactive properties of acellular extracellular matrix scaffold. *Tissue Eng Part A*. 2018;24(1-2):128–134.

58. Blázquez R, Sánchez-Margallo FM, Crisóstomo V, et al. Intrapericardial administration of mesenchymal stem cells in a large animal model: a bio-distribution analysis. *PLoS One*. 2015;10(3):e0122377. https://doi.org/10.1371/journal.pone.0122377